# Template-Assisted Chemical Vapor Deposited Spinel Ferrite Nanotubes

**ARTICLE** *in* THE JOURNAL OF PHYSICAL CHEMISTRY C · NOVEMBER 2010

Impact Factor: 4.77 · DOI: 10.1021/jp101099u

# Template-Assisted Chemical Vapor Deposited Spinel Ferrite Nanotubes

**Sandeep Kohli,*,† Patrick R. McCurdy,† Derek C. Johnson,† Jaydip Das,‡ Amy L. Prieto,† Christopher D. Rithner,† and Ellen R. Fisher†**

*Department of Chemistry, Colorado State University, Fort Collins, Colorado 80523, United States, and Department of Materials Science and Engineering, Virginia Tech University, Blacksburg, Virginia 24061, United States*

*Received: February 4, 2010; Revised Manuscript Received: September 14, 2010*

Ternary copper ferrite and copper cobalt ferrite nanotubes were deposited via a chemical vapor deposition process utilizing decomposing solid precursors under oxygen flow into anodic aluminum oxide templates heated to 450 °C. Extracted nanotubes were subsequently calcined at 450 °C for 12 h. Transmission electron microscopy, selected-area electron diffraction, energy dispersive spectroscopy, X-ray diffraction, and scanning electron microscopy were used to characterize the spinel nanostructured tubes. Copper and cobalt ferrite spinel phases were formed at 450 °C, which is significantly lower than previously reported, due to increased chemical reactivity of the constituents in the nanotubular structure. To the best of our knowledge, this is the first reported study of chemical vapor deposited copper ferrite spinel nanotubes at temperatures less than 700 °C.

Magnetic nanoparticles have been extensively studied for their potential applications in magnetic disk drives, spintronics, and biomedical applications.[1] Magnetic tubular structures offer the advantage of morphology-dependent properties, which can be controlled by tuning wall thicknesses, diameter, and length.[2,3] Although various growth methods are available for nanotubes and nanorods, template-based methods are becoming more prominent because nanotubes and nanorods of varying aspect ratios can be synthesized with relative ease.[4−6] Among nanotubes of magnetic materials, the synthesis of the Co and Cu ferrite spinel nanotubes reported herein has typically required temperatures in excess of 700 °C.[7] Several $MFe_2O_4$ (M = Co, Mn, Ni, Cu) nanotubes have been deposited using hematite nanotube/nanoring templates at 720 °C.[7] These low density hollow structures formed by these materials may find applications in biological applications where it is desirable to float magnetic materials in solutions.[8] $MFe_2O_4$ (M = Cu, Ni, Co) materials have also been investigated for their application as anode materials in all solid-state batteries.[9−11] Hence, it is desirable to have a low temperature commercial process that would employ low cost materials, have reduced thermal budget, as well as reduce reactivity with different parts of an end device or layers of other types of materials. Here, we report the template-assisted chemical vapor deposition (CVD) synthesis of ternary copper ferrite spinel ($CuFe_2O_4$) and copper cobalt ferrite spinel nanotubes at 450 °C. Notably, an extensive literature survey did not yield any previous reports presenting CVD of $CuFe_2O_4$ materials (thin films or nanomaterials).

## Experimental Details

Solid metal precursors—Cu(II) acetylacetonate ($Cu(acac)_2$, $Fe(acac)_2$, and $Co(acac)_3$)—were used to deposit nanotubes in a two-zone furnace. Commercially available anodic aluminum oxide (AAO) templates with pore diameters of 300 nm were used for all of the depositions. The AAO templates were held at a temperature of 450 °C, while precursors were decomposed in the upstream furnace zone. An oxygen flow rate of 100 sccm was maintained during this process to react with the metal precursors deposited inside the heated AAO template pores. The AAO templates with deposited reactants were held at this temperature for 2 h to allow precursors to react and maximize the removal of hydrocarbons in the precursor. Post deposition, the AAO templates were polished using fine emery paper to remove unreacted precursors or excess deposits. Subsequent soaking in a 6 M NaOH solution for 12 h dissolved the AAO templates. In addition to the nanotubes formed in the pores, a macroscopic CuO film deposits on the AAO template exterior surface that cannot be completely removed by either physical means or chemical dissolution as described above. The CuO waste product is therefore intermixed with the nanotubes once the AAO template is dissolved. This is discussed in more detail in subsequent sections of this Article and is also expected to occur for both Fe and Co as well.

The resulting nanotubes extracted from the template were rinsed repeatedly with distilled water and ethanol and were dried in an oven. The nanotubes were then calcined under air at 450 °C for 12 h to remove any hydrocarbon species left during synthesis or extraction procedures. A temperature of 450 °C (same as the substrate temperature during the deposition) was used because at this temperature the hydrocarbon components can be removed without inducing any chemical or morphological changes in the nanotubes. The synthesis products were analyzed using scanning electron microscopy (SEM) [JEOL JSM 6500F field emission microscope equipped with a Thermo Noran energy-dispersive spectrophotometer (EDS)], X-ray diffraction (XRD) [Scintag X-2 (Cu X-ray source)], and high-resolution transmission electron microscopy (HR-TEM) [Philips CM200 with a Princeton Gamma Tech Prism 2000 (EDS)]. It is important to note that the TEM images, corresponding SAED patterns, and EDS spectra are representative of the desired nanotube product, not of the macroscopic transition metal oxide waste products discussed above. However, the magnetic mea-

* Corresponding author. Fax: (970) 491-1801. E-mail: sandeep.kohli@colostate.edu.
† Colorado State University.
‡ Virginia Tech University.

10.1021/jp101099u 
Published on Web 11/02/2010

surements and XRD patterns, which are macroscopic characterization techniques, provide information regarding the synthesized product as a whole, that is, nanotubes and waste products. Significant effort was expended to mitigate the formation of the waste product through reaction optimization in addition to postsynthesis removal. Unfortunately, this proved difficult and met with limited success.

## Results and Discussion

Initially, CuO nanotubes were deposited by decomposition and vapor transport of $Cu(acac)_2$. The precursor deposited inside heated AAO template pores and reacted with oxygen to form CuO nanotubes. SEM images of the CuO nanotubes are contained in Supporting Information Figure S1. The images illustrate the uniform growth of the CuO nanotubes with a length of ca. 50 $\mu$m and an outer diameter of ca. 300 nm, consistent with the pore diameter and thickness of the AAO template. EDS spectra of the nanotubes (data not included) contained peaks at energies corresponding to Cu and O. A subsequent XRD analysis suggested that the nanotubes were monoclinic CuO.[12]

To synthesize the ternary ferrite spinel ($CuFe_2O_4$), AAO templates containing previously deposited CuO nanotubes were placed in the CVD reactor. $Fe(acac)_2$ was evaporated and deposited into AAO templates containing the CuO nanotubes. The subsequent reaction of $Fe(acac)_2$ and the CuO nanotubes in the presence of oxygen resulted in the formation of $CuFe_2O_4$ while retaining the nanotube morphology. As for the synthesis of the copper cobalt ferrite spinel, AAO templates containing previously deposited $CuFe_2O_4$ nanotubes were loaded in the CVD reactor and subjected to vapor transported cobalt, for which oxygen was the carrier gas and $Co(acac)_3$ was the cobalt precursor. XRD scans were performed on samples before and after dissolving the templates. The peaks in the XRD pattern (Figure 1) were indexed to monoclinic CuO[12] and cubic ferrite spinel structures.[13,14]

Figure 2 contains representative TEM images and a representative selected-area electron diffraction (SAED) pattern of the initial CuO nanotubes. The lower magnification TEM image illustrates the polycrystalline nature of the nanotubes with a diameter of ca. 300 nm and a wall thickness of ca. 40 nm, which was determined by measuring the darker contrast region at the edge of the nanotube. As is evident by the lower inset TEM image, the nanotubes are comprised of platelets on the order of 50 nm for which the SAED pattern (upper inset) has been indexed to monoclinic CuO. As the SAED pattern consists mostly of spots, it can be concluded that the platelets are larger crystals that are randomly oriented. Also, the EDS spectrum from the nanotubes (Figure 2b) indicated the presence of Cu and O as the only elemental constituents. The peaks for both Ni and C can be attributed to the TEM grid. Thus, the synthesis of monoclinic CuO nanotubes was confirmed and subsequently used as the backbone for the synthesis of $CuFe_2O_4$.

After the CuO nanotubes were reacted with $Fe(acac)_2$, forming the ternary ferrite spinel ($CuFe_2O_4$), substantial differences in the structure and morphology were observed when compared to the original CuO nanotubes. Figure 3a contains representative TEM images and a representative SAED pattern for the $CuFe_2O_4$ spinel nanotubes. The TEM image in Figure 3a demonstrates that the overall morphology, with the exception of a slight reduction in the wall thickness and grain size, remains unchanged. As is evident by the TEM image contained in Figure 3b, the nanotubes are comprised of platelets approximately 25 nm in diameter. EDS spectra from these nanotubes contain peaks representative of the presence of Cu, Fe, and O. The origin of Ni and C is the same as previously mentioned.

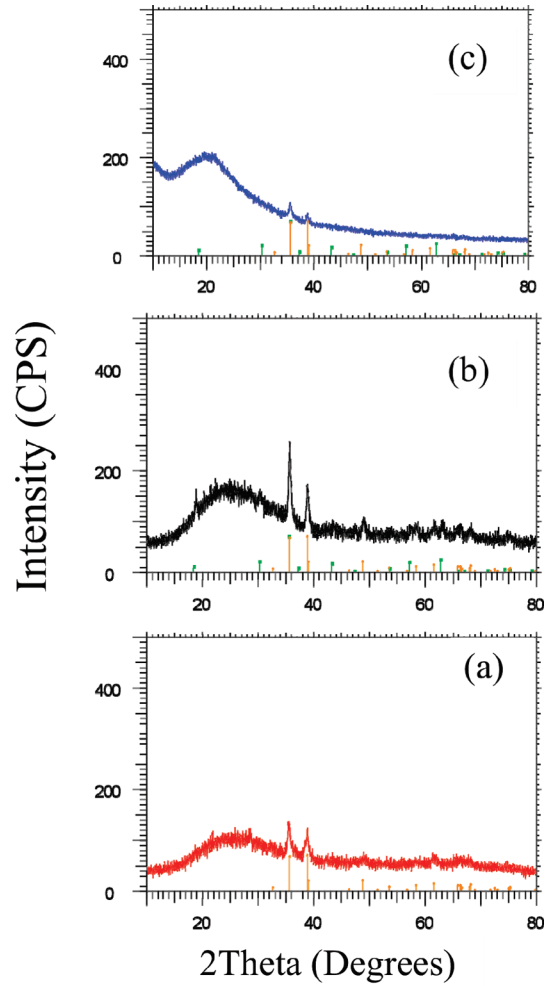


**Figure 1.** Raw XRD scans of nanotubes without any background subtraction. (a) CuO only, (b) Cu−Fe−O, (c) Cu−Co−Fe−O. XRD peaks were indexed to cubic ferrite spinel and monoclinic CuO. Orange and green bars show the peak positions for monoclinic CuO and cubic $CuFe_2O_4$, respectively, according to JCPDS data.

The reaction between the CuO nanotube backbone, Fe, and O is expected to lead either to the formation of a single Cu−Fe−O phase or to two separate phases of Cu−O and Fe−O. In the former case, the SAED pattern would be indexed to only a single copper ferrite phase. In the latter case, the SAED pattern would be composed of copper oxide and iron oxide phases. During the course of our investigation, evidence that supports the presence of separate Cu−O and Fe−O phases could not be found. This was accomplished by determining if the nanotubes contained CuO impurities. The most logical choice was to search for evidence of the CuO (111) plane in the SAED patterns because this particular reflection is the most intense, while not overlapping with that of a cubic structure with a lattice parameter, $a$, of approximately 8.37 Å. This is important because the structures for both iron oxide and the cubic copper ferrite spinel are cubic with approximately the same $a$ value. After examining multiple nanotubes from multiple reactions, evidence indicating the presence of monoclinic CuO was not found.

The SAED pattern (Figure 3a, inset) could only be indexed to a cubic phase with a lattice parameter, $a$, of approximately 8.37 Å. Both magnetite ($Fe_3O_4$) and cubic $CuFe_2O_4$ have the same crystal structure and associated lattice parameter.[14] The absence of CuO in the SAED patterns and presence of Cu, Fe, and O in the EDS spectra, however, clearly indicate the presence of a single cubic $CuFe_2O_4$ phase.[14] Although all of the rings

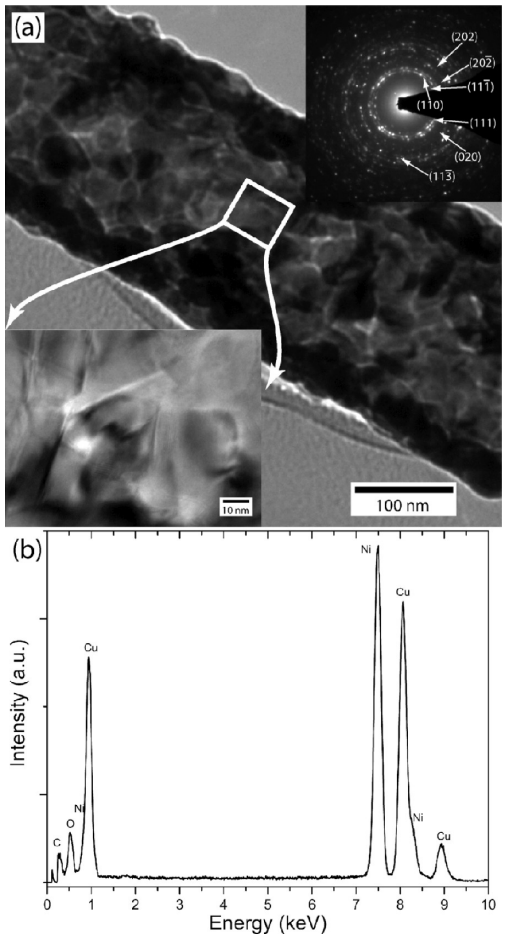


**Figure 2.** (a) Representative TEM images of the CuO nanotubes illustrating the morphology of the nanotubes and a representative SAED pattern (upper inset) of the nanotubes indexed to monoclinic CuO. (b) EDS spectra of CuO nanotubes with labeled peaks for Cu and O. The Ni and C peaks are from the TEM grid.

have been indexed, only the first seven are labeled for clarity. The reduction in platelet size is also evident in the SAED pattern. For the ternary spinel, the diffraction pattern consists mostly of rings, whereas the CuO pattern consists mostly of spots, indicating a reduction in the grain size. Despite the reduced grain size of the $CuFe_2O_4$ nanotubes, the platelets are still randomly oriented as in the CuO nanotubes.

The synthesis of $CuFe_2O_4$ is also supported by the HRTEM images in Figure 3b. The inset image is an enlargement of a pentagon-shaped platelet that is highlighted in the box of the main TEM image. The measured lattice spacing is consistent with the (311) plane of $CuFe_2O_4$, further confirming the indexed SAED pattern. It is important to note that because the synthesis of $CuFe_2O_4$ is a two-step process, CuO can still be indexed in the XRD pattern (Figure 1) of the ternary spinel nanotubes. As discussed in the Experimental Details, because XRD is a bulk analysis technique, it is likely that the CuO signal observed in the XRD pattern was from excess CuO present in the sample after the dissolution of the AAO template that could not be easily separated from the ternary ferrite spinel nanotubes. Typical porosity of these commercially available AAO templates ranges from 25−50%. With a wall thickness of about 50 nm, the overall mass of the nanotubes (300 nm diameter) is expected to constitute a much smaller fraction of the overall sample. Hence, in the XRD results, the signal from the CuO waste product overwhelms that from the poorly diffracting nanocrystalline $CuFe_2O_4$.

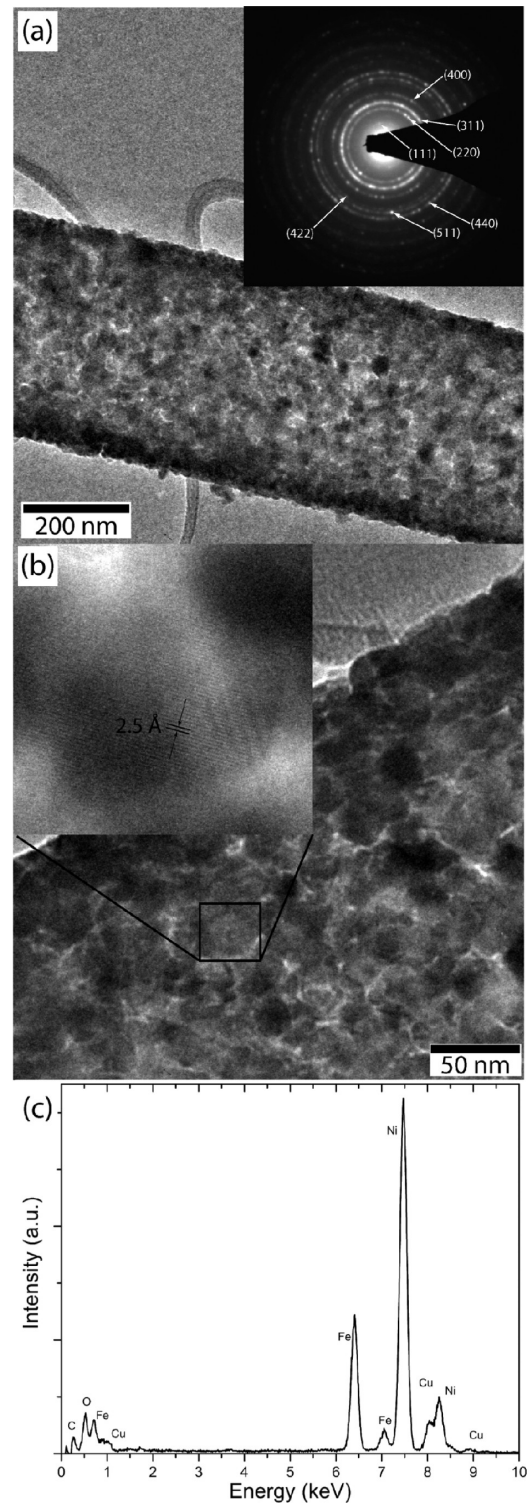


**Figure 3.** Representative TEM images and a representative SAED pattern of the as-synthesized $CuFe_2O_4$ nanotubes: (a) a lower magnification image demonstrating the polycrystalline nature of the nanotubes and a SAED pattern (inset) indexed to cubic $CuFe_2O_4$; and (b) HRTEM images reinforcing the polycrystalline nature of the nanotubes and reduction of the platelet size to 25 nm. The inset contains a HR-TEM image of a single platelet, highlighted in the boxed region, for which a measured *d*-spacing of 2.5 Å corresponds to the (311) plane of $CuFe_2O_4$. (c) EDS spectrum of $CuFe_2O_4$ nanotubes with labeled peaks for Cu, Fe, and O. The origin of Ni and C is the TEM grid.

Further changes in the morphology and elemental composition were observed after the $CuFe_2O_4$ nanotubes were reacted with Co precursors. Reaction of $Co(acac)_2$ with $CuFe_2O_4$ nanotubes

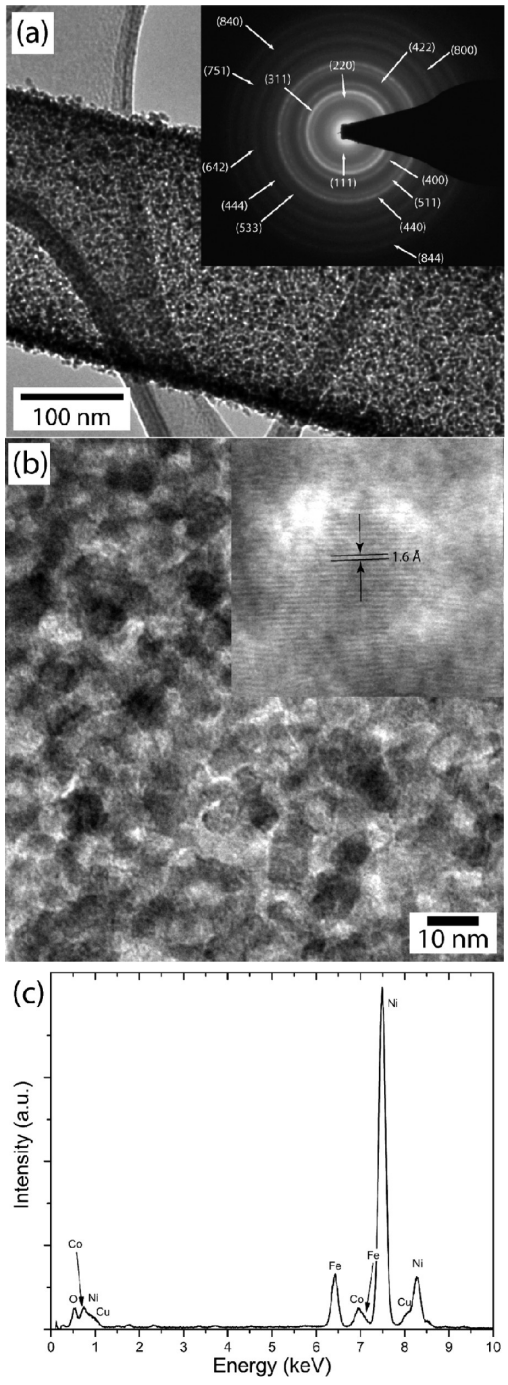


**Figure 4.** (a) Representative TEM image of the quaternary ferrite spinel nanotubes illustrating the dramatic change in morphology when compared to the CuO nanotubes. Inset is a SAED pattern indexed to cubic copper cobalt ferrite spinel. (b) HRTEM images illustrating the polycrystalline nature of the nanotubes and the sub-10 nm platelet size. Inset contains a platelet with a measured *d*-spacing of 1.6 Å, corresponding to the (511) plane. (c) EDS spectrum of copper cobalt ferrite spinel nanotubes with labeled peaks for Cu, Co, Fe, and O. The origin of Ni and C is the TEM grid.

leads either to the formation of a quaternary ferrite spinel ($Cu_{1-x}Co_xFe_2O_4$) or to two separate ternary phases ($CuFe_2O_4$ or $CoFe_2O_4$). The presence or absence of the quaternary phase could not be conclusively established with SAED because the crystal structures of $CuFe_2O_4$,[14] $CoFe_2O_4$,[13] and quaternary $Cu_{1-x}Co_xFe_2O_4$[15] are very similar. A representative SAED pattern of the nanotubes is contained in the inset of Figure 4a, demonstrating that in terms of crystal structure, the Cu−Co−Fe−O nanotubes are similar to the ternary ($CuFe_2O_4$) spinel nanotubes. As before, we did not find any reflections in the SAED pattern that could be attributed to phases of either copper oxide or cobalt oxide, even though CuO was again observed in the XRD pattern. This can again be attributed to the reasons stated above and will subsequently be discussed in more detail.

Although it could not be conclusively determined if the quaternary spinel was formed, TEM images in Figure 4a and b clearly demonstrate a further reduction in the grain size when compared to the ternary ($CuFe_2O_4$) spinel nanotubes. Figure 4a illustrates that the nanotube wall thickness has decreased, resulting in the nanotubes becoming translucent. This is a result of a further reduction in platelet size to sub-10 nm, which is apparent in Figure 4b. The reduction in the grain size of the cobalt-containing cubic copper ferrite nanotubes, as well as the presence of Co, Cu, Fe, and O in the EDS spectrum (Figure 4c), indicate the formation of quaternary $Cu_{1-x}Co_xFe_2O_4$, where a partial substitution of Cu for Co in the crystal lattice occurs, instead of the formation of two separate ternary phases ($CuFe_2O_4$ and $CoFe_2O_4$). Because of the extraordinary low formation temperature of the spinel phases, we sought to ensure that the nanotubes were chemically and structurally homogeneous. To that end, 10−20 nanotubes per composition, that is CuO, $CuFe_2O_4$, and $Cu_{1-x}Co_xFe_2O_4$, for multiple reactions were investigated. The selection aperture was focused either on a segment of a single nanotube, a majority of a single nanotube, or on multiple nanotubes. In all cases, the results were consistent, supporting the claim that the nanotubes are chemically homogeneous. Note, however, that without the ability to remove the unwanted waste product, the homogeneity of the nanotubes cannot be conclusively shown as that requires a macroscopic technique such as XRD.

Preliminary magnetization results in the case of $CuFe_2O_4$ and $Cu_{1-x}Co_xFe_2O_4$ indicated that these materials had low coercivity values of ca. 100 Oe. The slope of the high field component ($6.5 \pm 0.5 \times 10^{-5}$) for $Cu_{1-x}Co_xFe_2O_4$ in the linear region was lower than that for $CuFe_2O_4$ ($9.5 \pm 0.5 \times 10^{-4}$). This was indicative of more ferromagnetic contribution in the case of $Cu_{1-x}Co_xFe_2O_4$ as compared to $CuFe_2O_4$. More detailed experiments and analysis are planned to resolve the contribution of spinel to the magnetization results and will be reported in the future. Preliminary magnetization results are included in the Supporting Information (Figures S2 and S3).

Three important aspects of this work are the overwhelming presence of unreacted CuO in the XRD patterns, the remarkably low formation temperature of the spinel phases, and the reduction in both the grain size and the wall thickness of the nanotubes when exposed to Fe and Co. First, the discrepancy between the XRD patterns, a macroscopic characterization technique, and the electron microscopy studies can be explained by the observation that the macroscopic transition metal oxides (mainly CuO) that deposit on the surface of the AAO template cannot be separated from the nanotubes. Once the AAO template is dissolved, the macroscopic CuO is intermixed with the nanotubes. Because the nanotubes comprise a very small fraction of the overall sample, the presence of the CuO overwhelms the signal from the spinel phases when characterizing by XRD. As some of the nanotubes can be isolated on a TEM grid, elemental, morphological, and crystal structure data without the interference from the CuO waste product were obtained using these techniques, thereby verifying the composition of these nanoscale materials. Note that this was not accomplished without difficulty as macroscopic CuO was also present on the TEM grid,

sometimes incorporated in the AAO remnants that had not completely dissolved (data not shown).

Second, the conversion of the CuO nanotubes to the subsequent spinel phase at a remarkably low temperature, 450 °C, results from the nanoscale morphology of the tubes and high surface area of the nanoplatelets that comprise the nanotubes. Suppression of the formation temperature on the nanoscale has been observed previously for a number of chemical reaction systems.[16−21] The lack of a nanoscale morphology is the likely reason that the conversion of the macroscopic CuO to the corresponding spinel phase is inhibited. For this reason, the oxides persist even when the nanotubes are converted from CuO to $CuFe_2O_4$ and from $CuFe_2O_4$ to $Cu_{1-x}Co_xFe_2O_4$. Third, in considering the reduction of the nanotube wall thickness and platelet size when converting the CuO nanotubes to the subsequent spinel, we suspect that a decomposition and displacement reaction occurs in which the Cu is reactively removed from the nanotubes once introduced to the decomposed Fe and/or Co gaseous precursors, which are subsequently incorporated into the nanotubular structure. This synthesis approach has previously been employed to trap elements in an unstable oxidation state of a desired morphology and selectively remove transition metals from a host structure using various solid-state chemistry techniques.[22,23]

## Summary

Spinel ternary and quaternary nanotubes have been deposited using template-assisted CVD at 450 °C. It is likely that these ferrite structures (ternary and quaternary) are being formed at such low temperatures only as a consequence of increased nanoscale reactivity between the different elemental constituents. Increased nanoscale reactivity as well as size-dependent properties are well documented in the literature. To the best of our knowledge, this is first reported study of chemical vapor deposited copper ferrite spinel nanotubes at temperatures less than 700 °C. Application of template-assisted CVD of spinel nanotubes offers the unique possibility to deposit multicomponent and multilayered nanotubes of a wide variety of magnetic and nonmagnetic materials. Such experiments are currently being explored in our laboratories.

**Acknowledgment.** We would like to acknowledge financial support under NSF CHE-9977398, DMR-0114093, DMR-9870997, and CHE-9808024 for acquisition of instruments. We also acknowledge the assistance of Dr. John Chandler, Dr. Gary Zito, and the electron microscopy center at the Colorado School of Mines for the use of their HR-TEM.

**Supporting Information Available:** Additional figures. This material is available free of charge via the Internet at http://pubs.acs.org.

## References and Notes

(1) Emerich, D. F.; Thanos, C. G. *Expert Opin. Biol. Ther.* **2003**, *3*, 655–663.
(2) Escrig, J.; Bachmann, J.; Jing, J.; Daub, M.; Altbir, D.; Nielsch, K. *Phys. Rev. B* **2008**, *77*, 214421/1–214421/7.
(3) Bachmann, J.; Jing, J.; Knez, M.; Barth, S.; Shen, H.; Mathur, S.; Gosele, U.; Nielsch, K. *J. Am. Chem. Soc.* **2007**, *129*, 9554–9555.
(4) Lakshmi, B. B.; Patrissi, C. J.; Martin, C. R. *Chem. Mater.* **1997**, *9*, 2544–2550.
(5) Hernandez-Sanchez, B. A.; Chang, K. S.; Scancella, M. T.; Burris, J. L.; Kohli, S.; Fisher, E. R.; Dorhout, P. K. *Chem. Mater.* **2005**, *17*, 5909–5919.
(6) Shen, X. P.; Liu, H. J.; Pan, L.; Chen, K. M.; Hong, J. M.; Xu, Z. *Chem. Lett.* **2004**, *33*, 1128–1129.
(7) Fan, H.-M.; Yi, J.-B.; Yang, Y.; Kho, K.-W.; Tan, H.-R.; Shen, Z.-X.; Ding, J.; Sun, X.-W.; Olivo, M. C.; Feng, Y.-P. *ACS Nano* **2009**, *3*, 2798–2808.
(8) Nielsch, K.; CastaÒo, F. J.; Matthias, S.; Lee, W.; Ross, C. A. *Adv. Eng. Mater.* **2005**, *7*, 217–221.
(9) NuLi, Y. N.; Qin, Q. Z. *J. Power Sources* **2005**, *142*, 292–297.
(10) Lavela, P.; Tirado, J. L.; Womes, M.; Jumas, J. C. *J. Phys. Chem. C* **2009**, *113*, 20081–20087.
(11) Selvan, R. K.; Kalaiselvi, N.; Augustin, C. O.; Doh, C. H.; Sanjeeviraja, C. *J. Power Sources* **2006**, *157*, 522–527.
(12) 00-048-1548, JCPDS; International Center for Diffraction Data: Newton Square, PA, 2007.
(13) 00-022-1086, JCPDS; International Center for Diffraction Data: Newton Square, PA, 2007.
(14) 01-077-0010, JCPDS; International Center for Diffraction Data: Newton Square, PA, 2007.
(15) Mathew, T.; Shiju, N. R.; Bokade, V. V.; Rao, B. S.; Gopinath, C. S. *Catal. Lett.* **2004**, *94*, 223–236.
(16) Gole, J. L.; Burda, C.; Wang, Z. L.; White, M. *J. Phys. Chem. Solids* **2005**, *66*, 546–550.
(17) Tetley, T. D. *Biochem. Soc. Trans.* **2007**, *35*, 527–531.
(18) Guisbiers, G.; Buchaillot, L. *Nanotechnology* **2008**, *19*, 435701/1–435701/5.
(19) Sheehan, D. P. *J. Chem. Phys.* **2009**, *131*, 104706–11.
(20) Grabow, L. C.; Mavrikakis, M. *Angew. Chem., Int. Ed.* **2008**, *47*, 7390–7392.
(21) Rittner, M.; Abraham, T. *JOM* **1998**, *50*, 37–38.
(22) Bierman, M. J.; Van Heuvelen, K. M.; Schmeifler, D.; Brunold, T. C.; Jin, S. *Adv. Mater.* **2007**, *19*, 2677–2681.
(23) Ozawa, T. C.; Sasaki, T. *Inorg. Chem.* **2010**, *49*, 3044–3050.

JP101099U